Experiments and simulation of the growth of droplets on a surface (breath figures)

Daniela Fritter and Charles M. Knobler
Department of Chemistry and Biochemistry, University of California, Los Angeles, California 90024

Daniel A. Beysens
Service de Physique du Solide et de Résonance Magnétique, Direction des Sciences de la Matière, Centre d'Etudes Nucléaires de Saclay, 91191 Gif-sur-Yvette CEDEX, France

(Received 31 May 1990)

Detailed experiments are reported of the growth of droplets when water vapor condenses from a saturated carrier gas onto a hydrophobic plane substrate. We have investigated the effects of the carrier-gas flow velocity, the nature of the gas, the experimental geometry, and heat transfer through the substrate. Individual drops grow according to a power law with exponent $\mu=\frac{1}{3}$. At high flow velocities, the temperature of the substrate can rise significantly, which lowers the condensation rate and leads to lower apparent growth-law exponents. A self-similar regime is reached when droplets interact by coalescences. The coalescences continuously rescale the pattern, produce spatial correlations between the droplets, and accelerate the growth, leading to a power law with an exponent $\mu_0=3\mu$. The experiments are compared to predictions of scaling laws and to simulations.

I. INTRODUCTION

Nucleation and growth of droplets is a phenomenon of interest in many areas of technology and basic science. It can occur in bulk phases or on a substrate. The heterogeneous process is of importance in heat and mass transport and in thin-film technology; it is also of fundamental interest because the wetting properties of the surface play a crucial role because it is (at least in part) a two-dimensional process.

Breath figures (BF's), the pattern of droplets formed when liquids condense onto a glass surface, are a good model for the study of this phenomenon. They were initially[1,2] investigated as a means of detecting contamination of glass: on clean surfaces a dark continuous film forms; if the surface is contaminated by as little as a monolayer of oil, droplets form and the surface appears white because the droplets scatter light. Preliminary investigations of BF's by Beysens and Knobler[3] (BK) were performed by sending N_2 saturated with water vapor from a nozzle onto a glass slide that had been silanized, so that the contract angle for water was approximately 90°. The flux and the temperature difference between the saturated vapor and the slide were monitored, and the pattern of droplets was studied by small-angle light scattering and optical microscopy.

Four stages of growth were identified.

(i) In the earliest stage the surface coverage is low and droplets rarely coalesce. This stage is not observed in most experiments on solids because the droplets are too small to be resolved.

(ii) In the intermediate-time regime (Fig. 1) the droplets grow and coalesce, with no new visible droplets appearing on the bare space between them. The droplets are closely spaced and of almost uniform size, and the droplet pattern is self-similar in time, i.e., the statistical properties of the droplet pattern remain constant when the pattern is rescaled in size by a single time-dependent parameter. The scattered light forms an annular ring that shrinks in size as the length scale of the pattern increases. The surface coverage is nearly constant at a value of 0.55 and the time dependence of the average radius $\langle r \rangle$ of the droplets can be represented by a power law

$$\langle r \rangle \sim t^{\mu_0} . \tag{1}$$

The growth of single droplets between coalescences is also characterized by a power law

$$r \sim t^{\mu} . \tag{2}$$

BK found $\mu_0 \simeq \frac{3}{4}$ and $\mu \simeq \frac{1}{4}$.

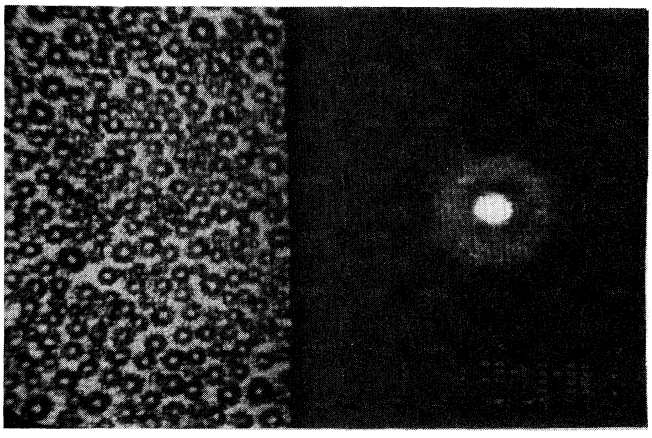

FIG. 1. Photos of BF growth: self-similar stage (ii), where the pattern of droplets is shown on the left and the annular light scattering pattern is on the right.

(iii) New droplets nucleate and grow in areas cleared by coalescence of original droplets. Initially, these new droplets appear singly in the middle of bare areas; at later times the bare areas become large enough that condensation occurring on them resembles that observed in the early-time regime.

(iv) In the long-time limit many generations of droplets coexist on the surface. If the surface is vertical, the largest droplets are overcome by gravity and slide down. New droplets then form in the spaces that have been cleared. This stage of the process is called steady-state dropwise condensation, and it has been investigated for many years by engineers interested in the accompanying heat transfer.[4]

Hysteresis of the contract angle can reduce the duration of the self-similar regime (ii) and cause the droplets to become anisotropic when they coalesce. Interconnected structures are formed, which develop into a pseudowetting film.

The properties of BF's have been the subject of several studies. Viovy, Beysens, and Knobler[5] investigated the scaling properties. They showed that μ_0 and μ are related through δ_p, the dimensionality of the drops, and δ_s, the dimensionality of the condensing surface

$$\mu_0/\mu=\delta_p/(\delta_p-\delta_s)\ , \tag{3}$$

and that

$$\mu=\frac{1}{\delta_p} \tag{4}$$

as long as vapor condenses on the substrate at a constant rate. Meakin and Family[6] have also demonstrated scaling for the growth rate of single droplets between coalescences, assuming a growth with exponent (ω) as

$$\frac{dr}{dt}=ar^{\omega}\ , \tag{5}$$

a form which implies a nonconstant condensation rate (see below).

Numerical simulations of droplet growth with coalescence were performed by Fritter *et al.*[7] They assumed that individual droplets grow with a power law and verified the relation (3) between μ and μ_0. A mechanism of single droplet growth by surface diffusion has been described by Rogers, Elder, and Desai;[8] their model gives $\mu=\frac{1}{4}$.

Droplet growth and coalescence have also been studied on substrates other than glass. In the early stages of vapor deposition, metal aggregates a few nanometers in size behave like liquid droplets and stages (i) and (ii) can be clearly seen. An analysis of such experiments[9] gives $\mu\simeq\frac{1}{3}$, $\mu_0\simeq 1$. The same exponents ($\frac{1}{3}$, 1) are found for the growth of water droplets condensing on liquid paraffin oil.[10]

Although the theoretical and experimental work carried out so far is in generaly good agreement, the value of the exponent μ_0 remains in question. In this paper we investigate systematically the parameters of growth (temperature, flow rate, geometry), using a nozzle and a chamber. Our attention will be confined mainly to the intermediate-time regime (ii), in which the statistical and dynamical properties are relatively simply characterized and are most interesting from the viewpoint of statistical physics. We will also address to some extent the early-time regime, specifically how the pattern might develop from some hypothetical initial configuration. One of our main results is that the value $\mu=\frac{1}{4}$ is the result of thermal effects in the nozzle experiments, where the condensation rate is very high. When the substrate temperature is held constant, $\mu=\frac{1}{3}$.

II. EXPERIMENT

A. Optics and image analysis

The optical setup has been described elsewhere.[11] It enables direct-space observation in the range 2–200 μm to be performed simultaneously with small-angle light scattering in the range 1500–15 000 cm^{-1}, the smallest wave number being determined by the width of the central beam.

Both patterns are recorded on videotape for further analysis. Individual frames from the experiments were digitized with an IP-512 Imaging Systems image processor. These data were used to calculate the average radius, the polydispersity, and the surface coverage as functions of the time. The structure factor was obtained by performing a radial average by computer about the central beam, and then subtracting the radial average of the corresponding intensity profile before condensation in order to eliminate the central beam. An analysis of digitized images and single-droplet growth was carried out for a few experiments to verify that the statistical properties of the droplet patterns developed in the same way under different experimental conditions. This analysis established that an experiment could be fully described by studying the kinetics of the ring collapse. (Details are given in the Appendix.) For self-similar pattern evolution (Fig. 2), the slope on a log-log plot of the ring radius ($q_{\max}$) against time (t) corresponds to the negative of the overall growth law exponent μ_0 (see below); the time is measured from the point at which condensation first becomes evident by a darkening of the direct-space image. It is convenient to define a time t_f required to deposit an arbitrary fixed amount of material on the substrate, which we have taken as that at which q reaches the value $q_0=3750$ cm^{-1}; t_f^{-1} is thus a condensation rate.

The growth of individual droplets was followed by measuring their diameters directly on the screen of a television monitor. The $q_{\max}$ obtained in this way was found to be identical with that obtained by treating the digitized frames, so direct measurement of the ring radius was generally used because the digital analysis is much more time consuming.

B. Substrate properties

Single Clay Adams precleaned Gold Seal microslides (3 in.$\times$1 in.$\times$ 1 mm) were left in a 10% hydrofluoric acid solution for 5 min, rinsed well with distilled water, and dried in an oven at 40 °C. Their surfaces were silanized[12]

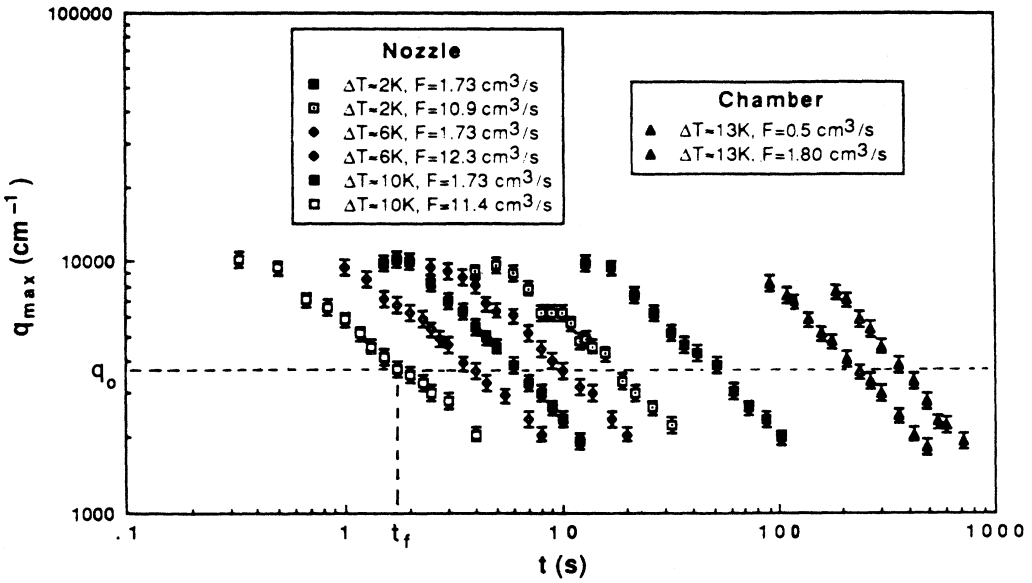

FIG. 2. Evolution of the ring radius q_{max} on a log-log plot for nozzle and chamber experiments at various temperatures and flow rates. The dashed lines show the definitions of the condensation rate t_f^{-1} and q_0. (The value 3750 cm^{-1} is arbitrary.)

by gently agitating each slide in a 0.10M solution of octadecyltrichlorosilane in hexadecane for 5 min and rinsing with toluene. The silane solution was discarded after it became 2 h old, which allowed up to 12 slides to be treated per fresh batch of solution.

The success of the treatment was checked by observing a water droplet deposited on the horizontal slide from a 10-$\mu\ell$ syringe. A video camera tilted about 7° from horizontal was aimed downward at the sessile drop so that a large-scale image of the droplet could be seen on the monitor. Direct measurements of the contact angle could be made with a protractor. The uncertainty in this measurement is estimated to be on the order of 2° or 3°. Both advancing and receding contact angles were measured; typical values for these were 100° and 90°, respectively, indicating a small degree of hysteresis. Slides whose surfaces exhibited a receding contact angle of less than 80° were not used in experiments.

C. Flow

Three different flow meters (Cole-Parmer 3216-45), which spanned volumetric flow rates from 0.3 to 15 cm^3 s^{-1}, were employed in the experiments. They were calibrated by measuring the volume of water displaced by nitrogen gas in a known time interval.

The carrier gas (nitrogen or helium) was passed through a 0.10-μm VC Millipore filter and one of the flow meters before bubbling through two flasks of distilled water at room temperature. The saturated vapor passed through a small, empty flask and then a large buffer volume (500 ml) in which the vapor temperature and relative humidity were measured with a hygrometer. For all experiments the gas in the buffer volume was essentially saturated with water (relative humidity $\geq 99\%$). After the saturated gas passed through the buffer volume, it flowed into the atmosphere until a bypass valve was turned to shunt it either through the nozzle or through the chamber.

The flow geometry in BF experiments performed with the nozzle is shown in Fig. 3(a). The nozzle, which was

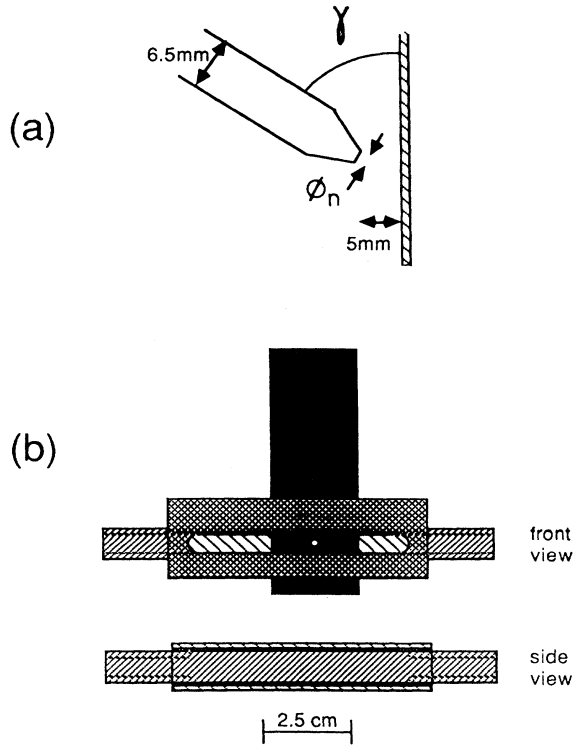

FIG. 3. Flow geometry in (a) nozzle and (b) chamber experiments. Front view of chamber shows copper block from temperature control assembly. Most of the nozzle experiments have been done with $\gamma = 60°$ and $\phi_n = 1.2$ mm.

made of glass, was mounted on a translation stage and its position was adjusted so that the droplets were centered in the field of view.

A small Plexiglass chamber through which vapor flowed parallel to the slide surface was also used. It was built to fit onto a slide [Fig. 3(b)]. Another slide was used as a window; it was attached to the cell with silicone rubber adhesive. The channel made by the slide, the window and the chamber walls was $6\times10\times50$ mm^3, and the tubes at the ends were 6 mm inner diameter.

D. Temperature control

The glass slide was held with nylon clamps to a copper block which was also in contract with a Peltier element (PE) (Fig. 4). A 2-mm hole drilled in the copper block allowed the laser light to pass through. The surface temperature T_s of the slide was measured to 0.1 K with a NiCr-NiAl thermocouple, which was wedged under one of the clamps holding the slide. T_s could be varied from -5 to 60 °C by adjusting the current applied to the PE from a dc power supply. The opposite side of the PE was held at a constant temperature by keeping it in contact with a copper cell through which water thermostated at about 15 °C circulated. The copper block, PE, and copper cell were clamped together and attached to a rigid support.

In the chamber experiments, the chamber was held to the copper block by rubber bands. Since it was inconvenient to measure T_s, the temperature T_{Cu} of the copper block at some distance from the slide was measured by wedging the thermocouple into a small hole in the Plexiglass next to the copper block. A calibration was made to relate the two temperatures.

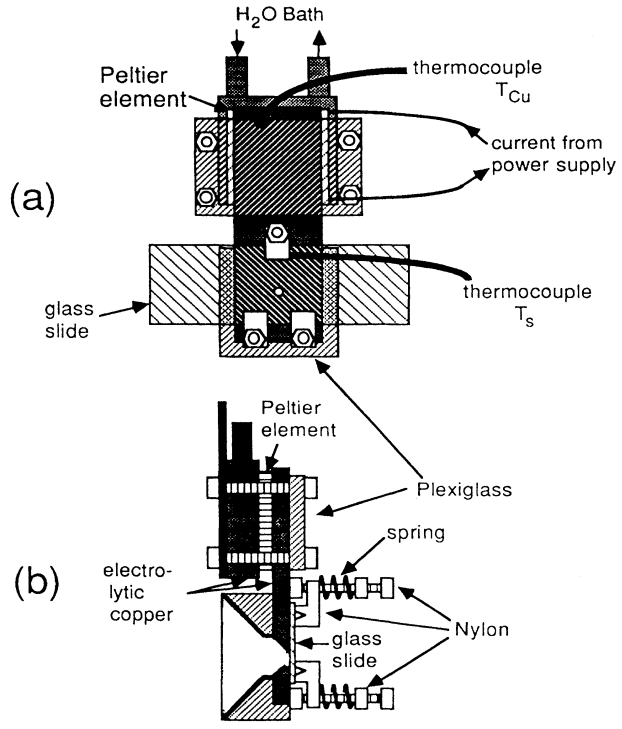

FIG. 4. Temperature control system. Bold lines through the Plexiglass and copper in the view (b) show a cross section where material has been removed to allow light scattered at large angles to pass through.

If even slight condensation has occurred on a newly prepared surface, and a BF experiment is done after this initial condensate has evaporated, enough impurities are left on the surface to alter the evolution of the droplet pattern significantly. The liquid will preferentially condense onto the impurities, disrupting the uniform carpet of condensate that would be observed on a fresh surface. This effect may alter the effective μ_0 measured from the light scattering,[13] thus only the results of experiments on a fresh surface were used. By translating the slide or chamber along its length so that a fresh portion appears in the area of observation, a maximum of six nozzle experiments or four chamber experiments could be performed per slide.

Experiments were also done to measure the temperature change at the point on the slide where condensation occurred directly. The thermocouple wire was placed in a small groove etched with hydrofluoric acid into one side of a slide. The thermocouple was protected from direct contact with the vapor by covering the groove with a thin coverslip. BF experiments were then carried out under the usual conditions while the temperature was monitored.

III. EXPERIMENTAL RESULTS AND DISCUSSION

In the following we will establish the characteristics of the pattern and investigate the relationship of μ_0 and condensation rate t_f^{-1} to the flow rate and to the systematic variations in the surface temperature during the condensation process.

A. Self-similarity

Digitized images were analyzed for several experiments carried out under various conditions; the following results are typical of the droplet pattern evolution during an experiment. (The data presented in this section were all taken from a single nozzle experiment in which the temperature of the water-saturated nitrogen gas was 23.6 °C, the initial temperature on the surface of the slide was 18.6 °C, and the flow rate of gas through the nozzle was 5.2 cm^3 s^{-1}.)

From the microscopic observations, it is found that between coalescences the diameters of individual drops obey a power law with $\mu\simeq0.26\pm0.05$ [Fig. 5(a)] and that the area-weighted average droplet radius

$$\langle r\rangle=\sum r^3\Big/\sum r^2 \tag{6}$$

also follows a power law with an exponent about three times that for individual drops between coalescences [Fig. 5(b)]. The polydispersity g, which we define as

$$g=[(\langle r^2\rangle-\langle r\rangle^2)/\langle r\rangle^2]^{1/2}\ , \tag{7}$$

with $\langle r\rangle^2=\sum r^4/\sum r^2$, and the surface coverage ϵ^2 can also be determined from the images, and their depen-

dence on time is shown in Fig. 6. These quantities level off at about 0.6 and 0.2, respectively.

The light scattered in the forward direction forms an annular ring and, as shown in Fig. 7, plots of the intensity I against scattering wave number q at different times can be made to coincide by plotting them as $I(q)/I_{\max}$ against $q/q_{\max}$, where $q_{\max}$ is the value of q at the maximum in the scattering. The decrease of $q_{\max}$ with time follows a power law [Fig. 5(b)] with an exponent -0.76 ± 0.05. From the scaling behavior of the structure factor it is apparent that the evolution of the droplet pattern depends on only a single length, which we can take as $q_{\max}^{-1}$. Furthermore, within the precision of the experiment $\langle r\rangle \sim q_{\max}^{-1}$ and $\mu_0=3\mu$.

The values of μ and μ_0 found in this experiment are in accord with those found by BK;[3] we will show later that μ_0 may take on a range of values from about 0.7 to unity, depending on experimental conditions (see Fig. 2). In all cases, however, measurements with different values of μ_0 were consistent with $\mu_0=3\mu$.

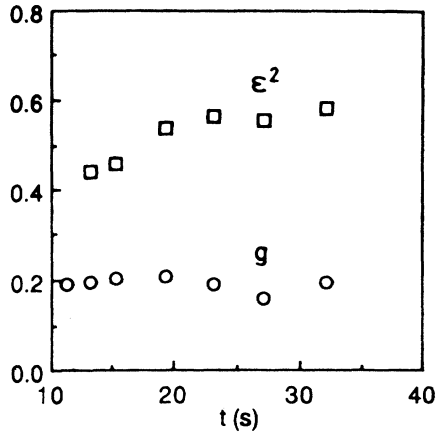

FIG. 6. Evolution of surface coverage ϵ^2 and polydispersity g during the intermediate regime of BF growth. Reliable measurements cannot be made at earlier times where there are many droplets with diameters smaller than 10 μm.

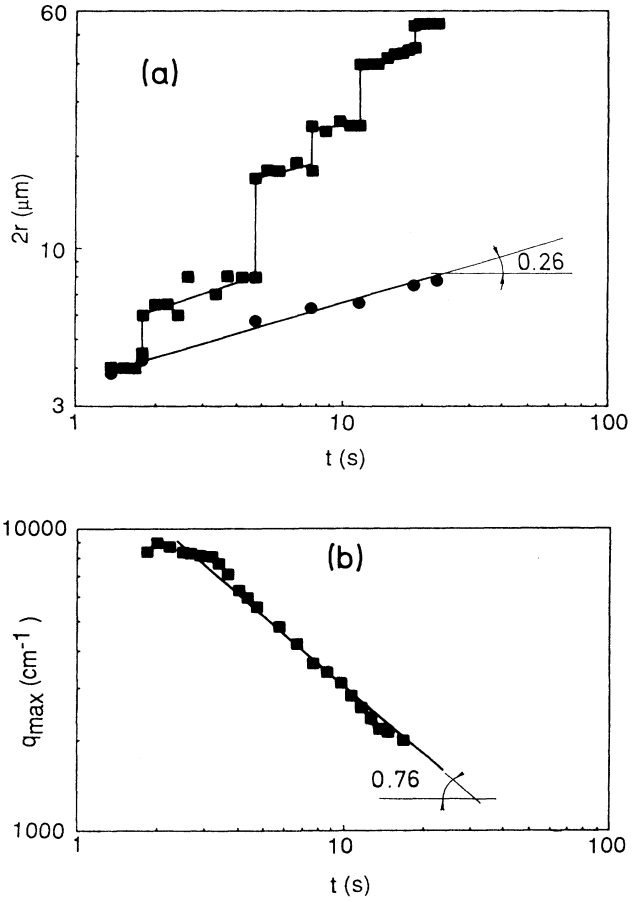

FIG. 5. Kinetics of BF growth in the intermediate regime. (a) Evolution of the diameter $2r$ of a single droplet. In the lower line the effect of coalescence has been removed. (b) Evolution of $q_{\max}\sim\langle r\rangle^{-1}$. Note that the negative value of the slope in (b) is about three times the slope in (a).

B. Flow-rate dependence

BK reported that the growth rate was roughly proportional to the volumetric flow rate F of the saturated gas directed to the surface. Log-log plots of t_f^{-1} against F showed[13] that the behavior was more complicated. At intermediate flow rates the slope was approximately unity, but seemed to be greater than 1 at low flow rates and markedly smaller than 1 at high flow rates. In order to understand this behavior we undertook a more detailed experimental study of the character of the flow and of its effect on the growth rate and also performed a simple steady-state theoretical analysis.

We take as our model a gas saturated with water flowing along a smooth wall that is maintained at a lower temperature. Liquid will condense on the surface and a depletion region, which we take to be stagnant, will be established near the wall. If the concentration of the water in the gas stream is small, w, the rate of mass transfer per unit area normal to the wall, is given by [14]

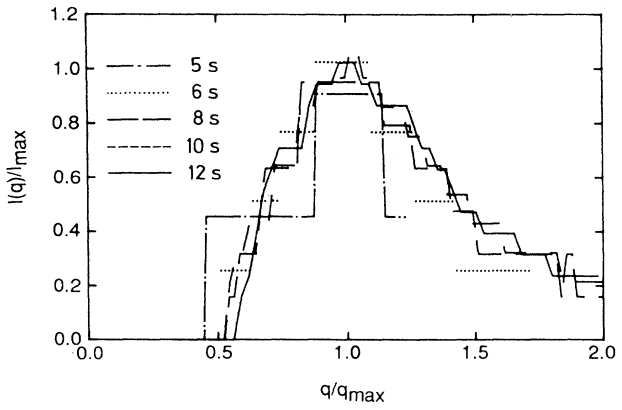

FIG. 7. Scaled structure factors $I(q)/I_{\max}$ vs $q/q_{\max}$ at several times during the intermediate regime.

$$w = D_{12}\Delta p / \delta R T \ , \tag{8}$$

where D_{12} is the diffusion constant of water in the carrier gas, Δp is the difference between the partial pressure of the water in the gas stream far away from the wall and the saturation pressure at the wall temperature, R is the gas constant, T is the mean temperature, and δ is the thickness of the depletion layer.

To evaluate δ, we consider the wall as a flat plate on which there is a temperature discontinuity. In this case the depletion-layer thickness can be related to the free-stream velocity u, the kinematic viscosity ν, and the Schmidt number $\mathrm{Sc} = \nu / D_{12}$ by[15]

$$\delta = (x\nu/u)^{1/2} / C\,\mathrm{Sc}^{1/3} \ . \tag{9}$$

In this expression x is the distance traveled past the edge of the temperature discontinuity and C is a constant, which is 0.33 if the velocity profile is unaffected by mass transfer at the surface.[16] A relation of identical form has been shown[17] to be applicable for normal flow onto a flat disk from a jet with x replaced by ϕ_n, the diameter of the jet, and C by a constant of order unity that depends on the disk diameter.

In our experiments we have measured the supersaturation in terms of ΔT, the difference between the temperature of the gas stream (T_v), and that of the surface (T_s) rather than Δp. A fit of the vapor pressure curve in the temperature range of interest leads to the relation

$$\Delta p / RT \propto \Delta T^{0.8} \ . \tag{10}$$

Combining Eqs. (8)–(10) gives an expression for the dependence on the flow rate of the time t_f required to deposit a fixed amount of material on the surface:

$$t_f^{-1} \propto w \propto (u^*)^{1/2} \Delta T^{0.8} D_{12} \ , \tag{11}$$

where $u^* = u / (\nu D_{12}^2)^{1/3}$. We will usually express the flow rate in terms of the scaled volumetric flow as $F^* = u^* A$, where A is the cross-sectional area of the flow stream, being careful to take A into account when we compare the chamber and nozzle experiments made with orifices of different size.

We can test the applicability of Eq. (11) to our experiments by plotting the product $(t_f \Delta T^{0.8} D_{12})^{-1}$ against $(F^*)^{1.2}$; such a plot is shown in Fig. 8(a). The measurements were performed in the chamber with N_2 and He as carrier gases; their properties are markedly different: for N_2, $D_{12} = 0.20\ \mathrm{cm^2\,s^{-1}}$ and $\nu = 0.14\ \mathrm{cm^2\,s^{-1}}$, while for He the values are 0.70 and 1.07 $\mathrm{cm^2\,s^{-1}}$, respectively. Supersaturations ranged from 2.9 to 18.8 K and flow rates from 0.17 to 9.1 $\mathrm{cm^3\,s^{-1}}$.

One sees that Eq. (11) provides a good representation of the flow behavior, except at the lowest flow rates. The depletion layer model should not be expected to hold under conditions where δ becomes comparable to the cell height. At very low flows essentially all the water can condense and we expect $t_f^{-1} \propto F$, which is consistent with the observations [Fig. 8(b)].

A similar set of studies with a 1.2-mm-diameter nozzle at supersaturations of 2, 6, and 10 K has also been performed. Here the comparison between the observed and predicted behavior was not as satisfactory because, as we show in Sec. III C, significant thermal effects are present that were neglected in the earlier studies of BF's.

C. Effect of temperature

The change in surface temperature during condensation can be estimated from a simple energy balance. We can write the heat flux q_c accompanying the condensation of the droplet as

$$q_c = h(T_v - T_s) \ , \tag{12}$$

where h is a heat transfer coefficient, and that conducted away to the copper block below the glass slide by

$$q_b = k(T_s - T_b) \ , \tag{13}$$

where k is the thermal conductivity of the glass divided by its thickness and T_b is the temperature of the lower

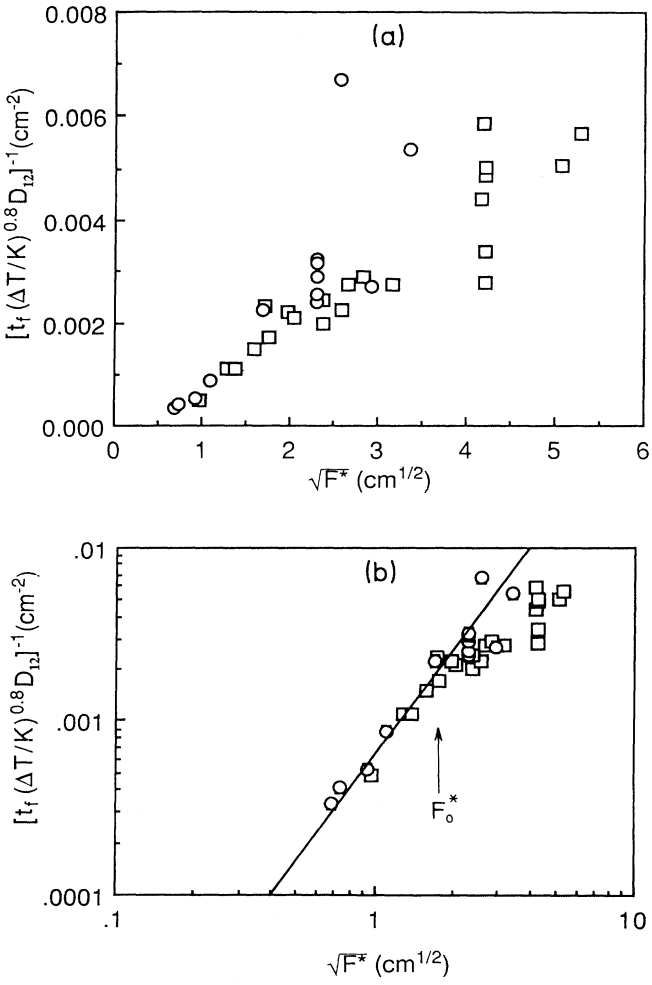

FIG. 8. Condensation rate t_f^{-1} dependence of flux F for chamber experiments with N_2 (□) and He (○) as carrier gases: (a) $(t_f \Delta T^{0.8} D_{12})^{-1}$ vs $\sqrt{F^*}$. (b) is a magnification on a log-log plot at small flux F^* showing a deviation for $F^* < F_0^*$, the value for which the depletion layer δ becomes comparable to the cell height.

glass surface, taken to be that of the copper block.

The amount of heat conducted through the glass before the flow of gas is initiated is small, so we can take the initial surface temperature (T_0) to be equal to T_b. At steady state, $q_c = q_b$, which leads to an expression for the relative change in surface temperature

$$\Delta T_s/\Delta T_0 = (T_v - T_{ss})/(T_v - T_0) = 1/(1+h/k) , \quad (14)$$

where T_{ss} is the steady-state temperature of the surface.

The heat-transfer coefficient can be estimated using the results of Sec. III B. We recognize that q_c is related to w by the enthalpy of vaporization ΔH:

$$q_c = w\Delta H , \quad (15)$$

from which we obtain

$$h = D_{12}\Delta H/\delta RT . \quad (16)$$

[For simplicity, in deriving (16), we have taken Δp proportional to ΔT rather than $\Delta T^{0.8}$. This makes no qualitative change in the results; the correct dependence can be employed in detailed calculations.]

We see from Eqs. (9), (14), and (16) that the change in surface temperature expressed as the departure of $\Delta T_0/\Delta T_s$ from unity should be proportional to $(u^*)^{1/2}$ and be independent of the supersaturation. Measurements of the steady-state temperature were carried out with N_2 carrier gas for three nozzle sizes and in the chamber. The results are consistent with those predicted by the calculation. Note that the temperature change depends on u rather than F. Thus, for measurements performed at the same volumetric flow rate, the temperature change is small in the chamber measurements, but very large in the experiments carried out with a 1.2-mm-diam nozzle.

The effect of the change in temperature on the growth measurements depends on the time required for the steady state to be achieved. If it is short, then the effect is only a systematic error in the supersaturation, which would not affect the growth-law exponent. On the other hand, if the temperature changes during the growth measurements, the varying supersaturation will be reflected in the exponent. Temperature-time measurement for experiments made at several supersaturations with two nozzle diameters are plotted in Fig. 9. The line drawn through the data points is the empirical expression

$$[T_s(t) - T_0]/(T_{ss} - T_0) = 1 - e^{-t/t_d} \quad (17)$$

in which $t_d = 5.5s$, which corresponds to a typical diffusion time for the transfer of heat through the slide. In these experiments the steady-state temperature is reached in about 20 s, a time comparable to the period during which measurements of the growth rate had been performed.

The effect on the growth rate of this systematic variation in the temperature can be estimated. The volume of condensate on the surface can be written

$$V = (2\pi/3)\sum r^3 = (2\epsilon^2/3)A_s\langle r\rangle , \quad (18)$$

where A_s is the total surface area and the equality follows from the definitions of the area-averaged radius $\langle r\rangle$ and the surface coverage ϵ^2.

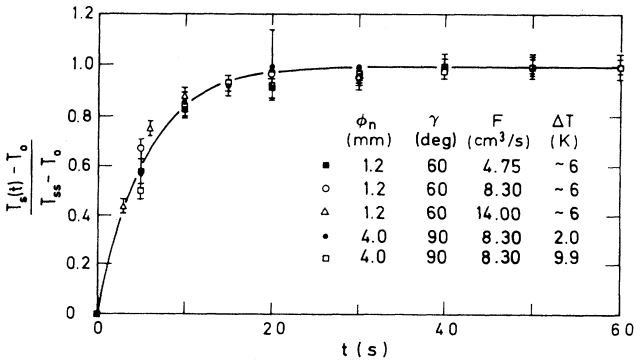

FIG. 9. Rise in slide surface temperature for nozzle experiment (N_2 as carrier gas) after condensation is initiated. Large error bar is typical for smallest ΔT.

Applying Eq. (11), we can write the instantaneous condensation rate as

$$\frac{dV}{dt} \sim \frac{d\langle r\rangle}{dt} = BF^{1/2}[T_v - T(t)]^{0.8} , \quad (19)$$

with B a constant. If $T_s(t)$ is represented by Eq. (17), $\langle r\rangle$ can be obtained as a function of t by numerically integrating Eq. (19). The result is shown in Fig. 10 for $\Delta T_s/\Delta T_0 = 0.5$, a value typical of many of the nozzle experiments. Note the asymptotic behavior: at small t, $T(t) \sim T_0$ and $\langle r\rangle \sim \Delta T_0^{0.8} t$; at large t, $T(t) \sim T_s$ and $\langle r\rangle \sim \Delta T_{ss}^{0.8} t$. These bounding lines are also shown in Fig. 10 and exhibit unit slope.

In a BF experiment the experimentally accesible values of q_{max} span about an order of magnitude, and if these measurements are taken during the transition period in Fig. 10, $\langle r\rangle$ (or q_{max}^{-1}) will appear to follow power-law growth with an exponent less than unity. There are primarily two factors that influence the apparent μ_0: the

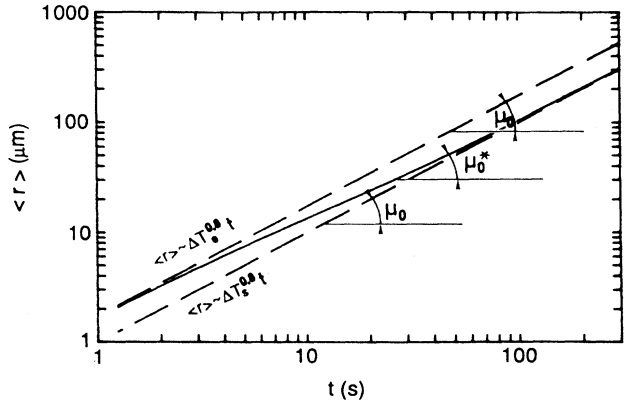

FIG. 10. Droplet radius evolution ($\langle r\rangle$ or q_{max}^{-1}) for a typical nozzle experiment when thermal effects are important [$\Delta T_0/\Delta T_S \simeq \frac{1}{2}$]: instead of exponent μ_0 it is $\mu_0^* < \mu_0$ that is measured.

value of $F^{1/2}\Delta T_0^{0.8}$ determines the position of the upper limiting line in Fig. 10 (and thus the time range in which measurements are made), while the separation between the limiting lines is an increasing function of $F^{1/2}\Delta T_0^{-0.2}$. At high F the temperature of the substrate rises significantly during condensation, i.e., ΔT decreases and the condensation rate slows.

In conclusion, in experiments in which the change in surface temperature is negligible, $\mu_0=1$, in accord with the scaling analysis. The previously reported lower values of the exponent are associated with experiments in which there was a significant rise in surface temperature. This temperature change was also the cause of the observed saturation of t_f^{-1} with increasing flow rate.

IV. COMPARISON BETWEEN EXPERIMENTS AND NUMERICAL SIMULATIONS

A. Background

Many simulations of droplet or aggregate growth including coalescence have been carried out, but they have usually explored the last, steady state of condensation[18–20], or have been too limited in extent[21] to be of use in describing the self-similar growth regime in which we are interested. We will compare our experiments to three numerical simulations. The first is that of Fritter *et al.*[7] and is concerned with the evolution of a two-dimensional pattern of droplets from an initial random configuration. The growth law of an individual droplet (i) between coalescences is assumed to be

$$r_i = r_0 t^{\mu} , \tag{20}$$

where r_0 is evaluated at each step. The second simulation (MF) is due to Meakin and Family,[6] who took the rate of growth between coalescences to be given by Eq. (5) with ω constant throughout the process. Briscoe and Galvin[22] have reported simulations with an essentially identical model. The third simulation (FM), also due to Family and Meakin,[23] is based on a model in which the droplet growth occurs by a "rain" of monomer droplets.

In all the simulations the radius of the droplet formed by a coalescence is calculated by mass conservation:

$$r_i = (r_{i-1}^{\delta_p} + r_{i-1}'^{\delta_p})^{1/\delta_p} . \tag{21}$$

The new droplet (i) is placed at the center of mass of the two original droplets ($i-1$). Periodic boundary conditions are used to eliminate edge effects. In the simulations described here δ_p was taken as 3.

B. Comparison of experiments with simulations

This simulation of Fritter *et al.* starts from sites placed randomly on a unit square. The sites were taken as the centers of equal-size disks whose radius was chosen empirically so that there would be some overlaps (i.e., coalescences) in the first step. The original simulations were carried out for a maximum of 10 000 droplets at the start; here we will report results obtained for 100 000 drops, for which the statistical fluctuations at late times are much smaller. Initial configurations at relatively high coverages were generated by placing the disks sequentially at random positions and rejecting coordinates that would result in overlaps. This procedure is quite time consuming for coverages in excess of 45% and an alternative was also investigated in which droplets were initially placed on either a 100×100 square or hexagonal lattice. The system was then distorted by moving each disk a random distance and direction within a circle whose size was defined by the closest packing radius.

In some of the simulations, polydispersity was introduced into the initial droplet distribution by choosing droplet radii with a Gaussian probability about the average radius. When the initial configuration was that of a distorted lattice, an upper bound to the radius was set by the requirement that disks fit within the circle defined by the closest packing radius; the lower bound was then chosen to make the distribution symmetric.

1. Growth laws

At each step, the radius of each droplet is increased according to Eq. (20), or

$$r_i^{\text{new}} = r_i^{\text{old}}(t_{\text{new}}/t_{\text{old}})^{\mu} = r_i^{\text{old}}(1+\delta t/t_{\text{old}})^{\mu} . \tag{22}$$

It is convenient to carry out the simulations in terms of a reduced time variable $\tau=(t/t_1)^{\mu}$, which makes the simulation independent of the value of the power-law exponent for single-droplet growth, and to express the radius as a reduced quantity $\rho=\langle r\rangle/\langle r\rangle_0$, where $\langle r\rangle$ is the area-weighted radius, and $\langle r\rangle_0$ is its value at the initial time. Figure 11(a) shows the behavior of $\log\rho$ as a function of $\log\tau$ for a system that was initially monodisperse, prepared at an initial coverage of 3%. It is evident from Fig. 11(a) that there is an initial period during which the slope is unity, corresponding to single-particle power-law growth ($\langle r\rangle\sim t^{\mu}$) followed by a transition to a slope of 3 (3μ growth). This characteristic crossover from single-particle to coalescence-dominated growth is observed in all the simulations, regardless of the choice of initial conditions, polydispersity, or procedure for drop replacement at coalescence. It is also unaffected by dimensionality, as shown by experiments and simulations of BF growth on a one-dimensional substrate:[24] there is always a crossover from $\rho\sim\tau$ to $\rho\sim\tau^{\mu_0/\mu}$, this exponent being related to the droplet and substrate dimensions by Eq. (3).

Plots of the coverage ϵ^2 and polydispersity g against τ are given in Fig. 11(b). After an initial rise, ϵ^2 levels off at a value of 0.57, and the time t_0 at which $\epsilon^2\approx0.4$ corresponds to the change from single-droplet to coalescence-dominated growth. The polydispersity also shows this transition. As can be seen in Fig. 11(b), it rises through a small maximum to a plateau at a value of 0.16, where the transition in growth law takes place.

Although the transition from the exponent μ to 3μ in the power-law growth of the average radius was difficult to observe in the original experiments on clean, silanized glass slides (Figs. 2 and 5), it was inferred from experiments in which there were isolated impurities on the surface of the slides[13] and it has been confirmed in studies of the growth of droplets on the surface of a liquid.[10] The appearance of a self-similar growth regime is also a natu-

ral result of the power-law growth and the coalescence process, which act together to preserve self-similarity.

The quantitative results of the simulations agree remarkably well with those found in the experiments. It is notable that the plateau value of the coverage (57%) is close to the "jamming limit," the maximum coverage obtainable when monodisperse disks are placed randomly and sequentially on a two-dimensional surface with the requirement that there be no overlap. This process of random sequential adsorption has been much studied. The jamming limit in two dimensions has not been computed analytically, but Hinrichsen, Feder, and Jossang[25] determined the value 0.547 ± 0.003 from computer simulations. It should be noted that Rose and Glicksman[4] suggested that the limiting coverage in droplet condensation is the jamming limit, and that Briscoe and Galvin[22] report a limiting coverage of 0.55 in their simulations (although they did not use periodic boundary conditions). The value of g in the self-similar regime obtained from the simulations is slightly less than 20%, as observed in the experiments [Figs. 6 and 11(b)].

2. *Size distributions*

The distributions of droplet sizes found in the simulations are bimodal, Fig. 12(a). The small peak at low r results from a few droplets that do not coalesce and therefore grow much more slowly than $\langle r \rangle$. In general, the small droplets do not contribute much to the (area-weighted) average properties, but as coalescences reduce the number of large droplets, the effect of the small droplets can be seen. As one might expect, the bimodality increases with increasing initial polydispersity. In simulations in which the initial polydispersity is greater than 5%, the maximum in g at early times becomes more pronounced and the plateau region at late times becomes less

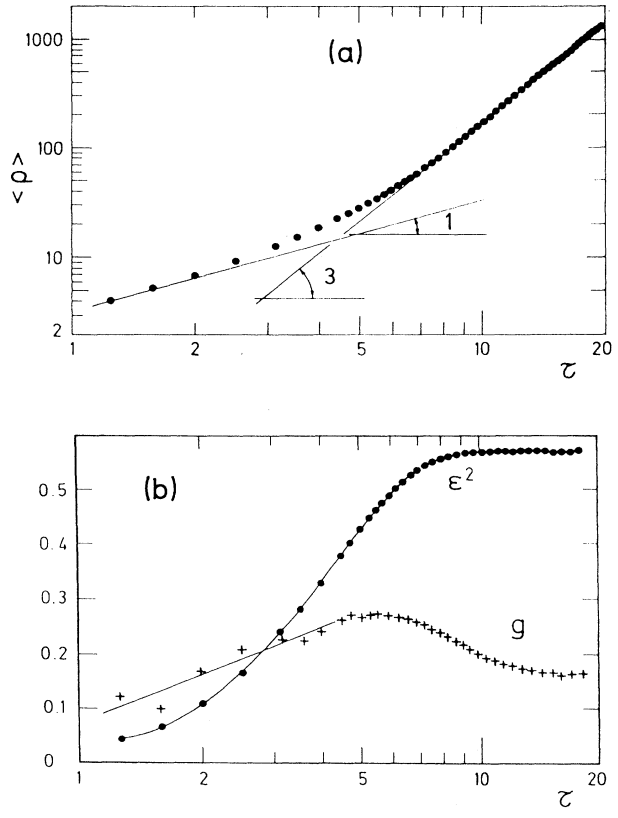

FIG. 11. (a) Log-log plot of ρ against τ for a random initial condition with 10^5 disks and a coverage of 3%. The system was initially monodisperse. (b) Coverage ϵ^2 and polydispersity g against τ for the systems shown in (a) (semi-log plot).

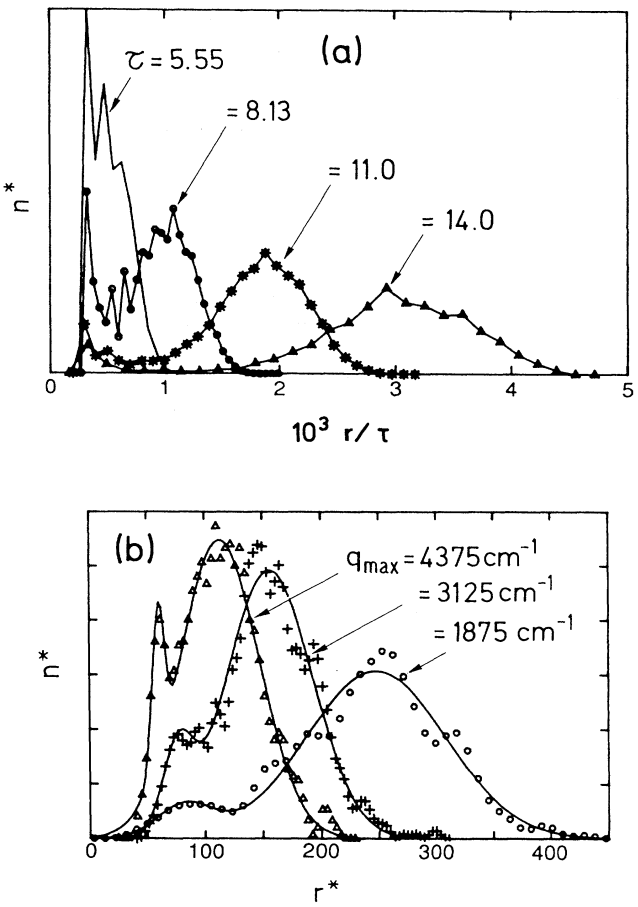

FIG. 12. (a) Distribution of droplet sizes at four times during the simulation for a random initial condition of 10^5 monodisperse disks with 3% coverage. The abscissa has been divided by τ to factor out growth not due to coalescence, and the ordinate has been normalized to give an area of unity under each curve: $n^*=n/(Ndr/\tau)$, with dr the bin size, which is different for each curve, and N the total number of droplets. (b) Size distributions of droplets in an area of 170×260 μm^2. The bin size is 0.25 μm. Treatment and normalization are as follows: $\triangle$, subjected to three-point smoothing; +, subjected to five-point smoothing, $\circ$, subjected to five-point smoothing after the bin size was increased to 0.75 μm. The normalization $[n^*=n(Ndrq_{\max}^{1/3})^{-1}$, $r^*=rq_{\max}^{1/3}]$ is equivalent to that shown in (a) (these measurements were made from experiments in which $\mu_0=1$ so $\tau\sim t^{1/3}\sim q_{\max}^{-1/3}$). The curves drawn through the points are least-squares fits of the raw data to two arbitrary normal distributions.

well defined, effects that can be attributed to the breakdown of self-similarity caused by the presence of a significant fraction of droplets whose properties are not rescaled by coalescence.

Experimental droplet distributions are difficult to determine because the number of droplets in the field of the microscope is small. We have obtained distributions corresponding to the times at which $q_{\max}=4375$, 3125, and 1875 cm^{-1} by combining, respectively, the results of 4, 10, and 13 individual experiments. These distributions, which are shown in Fig. 12(b), have an asymmetric appearance, suggesting that they also exhibit the bimodality found in the simulations. We therefore considered the possibility that the distributions could be represented by the sum of two Gaussians. Each size distribution was plotted as a Q-Q plot[26] (the mixture quantile versus the unit normal quantile of the cumulative normalized probability), which displays the data as a straight line if the distribution is normal and as a curve that shows a transition from one straight line to another if the distribution is composed of two normals. Figure 12(b) shows curves obtained from a least-squares, six-parameter fit of the raw data to two arbitrary normal distributions that are consistent with the Q-Q plots. Superimposed on these curves are the same data that have been smoothed to a degree for the best representation by the least-squares curves.

3. *Pair correlation function*

A necessary condition for self-similarity is the scaling behavior of the structure factor, which is indicative of an underlying scaling of the pair correlation function. The average distance between disk centers is proportional to $N^{-1/2}$, where N is the number of droplets. This provides us with a characteristic length; we define a reduced distance $r^*=rN^{-1/2}$, where r is the radial distance from the center of a drop. The pair distribution function $g(r^*)$ of the center-to-center distances is shown as a function of r^* in Fig. 13 for different times during the simulation in which the initial disks were of negligible radius and randomly placed. At the start of the simulation, there is no correlation between the droplets and $g(r^*)$ is unity. As coalescences occur, the short center-to-center distances are preferentially eliminated and a short-range cutoff appears in the distribution function. At the same time, local order develops, as evidenced by the peak that arises in $g(r^*)$. As the system enters the regime in which the 3μ growth law applies, the maximum in the peak increases and there is evidence of a second peak, indicating that the correlation is increasing. At longer times, the distribution function approaches the $g(r^*)$ for systems in which the coalescence mechanism is well developed.

The behavior in other simulations is comparable; once the 3μ growth is well established, $g(r^*)$ does not change and the structure is therefore self-similar. The development of this local order seems to be due to an interaction which, in contrast to the hard-sphere model, should be infinitely attractive at the point of contact.

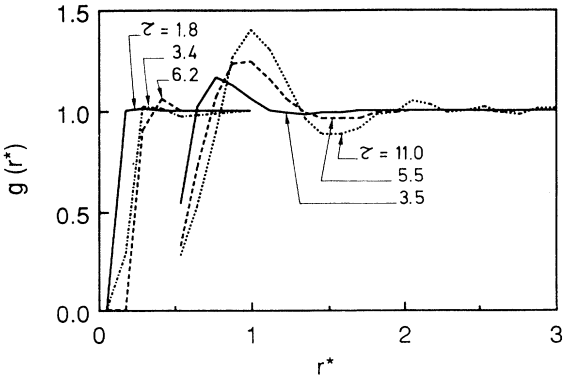

FIG. 13. Pair distribution function $g(r^*)$ against $r^*=rN^{-1/2}$ at several times during the simulation for an initial random condition of 10^5 monodisperse disks with 3% coverage ($\tau=3.5,5.5,11$). Results of the simulation for an initial random condition of 10^4 monodisperse disk with 0.3% coverage are also shown ($\tau=1.8,3.4,6.2$). These τ's are not directly comparable since the initial coverages at $\tau=1$ are different; however, at early times $\rho\sim\tau$ and $\epsilon^2\sim\tau^2$, and τ in the simulation with 10^4 initial disks may be rescaled, or multiplied by a factor $(\frac{0.3}{3})^{1/2}$, to correspond to the τ's in the simulation with 10^5 initial disks.

C. Comparison with the MF and FM simulations

Coalescence is the process which produces scaling, and both simulations MF (Ref. 6) and FM (Ref. 23) report only the stages where coalescences are important. A comparison with the early experimental stage is thus not possible.

In contrast to our simulation, the MF simulation is based on a mechanism in which the growth of a droplet is proportional to its surface area:

$$\frac{dV_i}{dt}=2\pi r_i^2\frac{dr_i}{dt}=a2\pi r_i^2 , \tag{23}$$

with a constant. This is simply Eq. (5), with $\omega=0$, and leads to $\mu=1$, not in agreement with our experimental value. (In Ref. 22, the value $\omega=\frac{1}{2}$ has been arbitrarily chosen, which leads to $\mu=\frac{2}{3}$, a result which also disagrees with our experiments.) In fact, the disagreement comes from the basic assumption (23), which leads to a rescaling of the prefactor of the growth law as a result of coalescence, not a rescaling of the exponent.

The FM simulation is based on a "rainlike" process, where at each step droplets of identical radius are added to the substrate at random positions. Those that land on existing droplets are incorporated into them. The resulting droplet size distribution has the form of a broad power-law decay with a superimposed bell-shaped distribution centered at the mean cluster radius $\langle r_c\rangle$. It is possible that the late stages, where many families of droplets have nucleated, correspond to this process.

V. CONCLUSION

With the completion of this study, we can reasonably state that the temperature and flow rate dependence of

the growth of BF's are well understood. The growth rate is seen to be dominated by the supersaturation ratio and a bulk depletion layer parallel to the substrate. Quantitative predictions have been made that fit the experiments.

The latent heat of condensation of water is so high that at high flow rate the temperature of the substrate can be affected, such as in nozzle experiments where the incoming flux is concentrated on a small region. The analysis of this phenomenon leads to a time-dependent condensation rate, with a modified growth law that can lead to a lower apparent exponent.

The details of the mechanism of growth of single droplets between coalescences have not at all been addressed. From preliminary experiments it appears that many phenomena are in competition: direct condensation at the surface of the drops, diffusion at the surface of the substrate, and thermomechanical effects inside the droplets.

ACKNOWLEDGMENTS

This work was supported in part by NATO Grant No. 86-0658 and by National Science Foundation Grant No. CHE-89-02354.

APPENDIX: STRUCTURE FACTOR AND STATISTICAL PROPERTIES

The intensity profile of the small-angle light -scattering results from the interference of light rays diffracted by the droplets, and is thus determined by the average structural or static properties of the droplet ensemble.[27] Consider a plane wave (monochromatic, coherent electromagnetic radiation) incident on an assembly of scattering elements. If the scattering matter is confined to N domains of similar shape and size in which the density of scattering elements is constant, the structure factor $[S(q)]$ can be written as the product

$$S(q)=NJ(q)[F(q)]^2 , \tag{A1}$$

where the form factor $[F(q)]^2$ describes the intensity pattern from one such domain, and the interference factor $J(q)$, which accounts for the interference of radiation scattered by the domains, is given by

$$J(q)=\frac{1}{N}\sum_{j,k}\exp(i\mathbf{q}\cdot\mathbf{R}_{jk}) . \tag{A2}$$

Here $\mathbf{R}_{jk}$ is the vector between the centroids of domains j and k and $\mathbf{q}$ is the transfer wave vector. In an ensemble of points, $J(q)$ is the sum of many terms, and the resulting function may or may not exhibit a maximum. If there is no spatial correlation, all lengths and orientations of R_{jk} are equally likely, and the maxima from each pair of sites will interfere to give a uniform intensity (excepting $q=0$).

In BF's, the arrangement of droplet centers can be described as an amorphous lattice[26] in which there may be some degree of short-range order among the sites, although they are otherwise randomly arranged. For an isotropic lattice, there is no preferred orientation of sites and $J(q)$ is radially symmetric about the axis of incident radiation. If the short-range order extends to distances such that there is a greater than average probability that neighboring sites are separated by the mean nearest-neighbor distance $\langle R_{\mathrm{NN}}\rangle$, then $J(q)$ exhibits a maximum in the form of an annular ring, whose dimension is defined by the wave number $q_{\max}$ which satisfies

$$q_{\max}=\frac{2\pi}{\langle R_{\mathrm{NN}}\rangle} . \tag{A3}$$

In general, for an assembly of similarly sized, compact domains of average size $\langle r\rangle$, $F(q)$ decreases from maximum intensity at $q=0$ to practically zero intensity at $q\langle r\rangle\approx 4.5$. Thus at small q, where $F(q)$ is still slowly changing, $S(q)$ will reflect $J(q)$, or the effect of interference between domains; at large q, where $J(q)$ is finite, $S(q)$ will be controlled by the rapidly vanishing $[F(q)]^2$, which is determined by the size distribution of the domains. The shape of $S(q)$ will thus be different for different values of $\langle r\rangle$ in the form factor, although the position of the maximum in $S(q)$ is essentially the same as $q_{\max}$.

The shape of $S(q)$ is thus dependent on the average statistical properties of the domain configuration. The effect on $S(q)$ as the surface coverage ϵ^2 is varied may be predicted. At high packing densities, the domains are crowded together and, since they are not allowed to overlap, there will be a short-range correlation between neighboring domains as discussed before. As the packing density is decreased, the short-range correlation fades as the position of an individual domain becomes less restricted by the location of its neighbors. The maximum in $J(q)$ becomes less pronounced.

The value of the size polydispersity g has a significant effect on the structure factor when the packing density is relatively high: the distribution of center-to-center distances around $\langle R_{\mathrm{NN}}\rangle$ becomes flatter and broader with increasing g, which results in a weaker maximum in $J(q)$.

Thus small packing densities and high polydispersities weaken the spatial correlation and therefore the maximum in $S(q)$. In fact, Hosemann and Bagchi[27] show that for domain configurations in which the difference ϵ^2-g is less than approximately 0.10 the degree of spatial correlation is too low to observe a maximum in $S(q)$, which instead decreases monotonically with increasing q. The fact that one sees a well-defined annular ring in the light scattering profile of a BF in the intermediate regime indicates that here we should find (ϵ^2-g) to be significantly higher than 0.10.

[1]J. Aitken, Nature **86**, 516 (1911); **90**, 619 (1913); Lord Rayleigh, Nature **86**, 416 (1911); **90**, 436 (1912).

[2]T. J. Baker, Philos. Mag. **44**, 752 (1922); R. Merigoux, Rev. Opt. **9**, 281 (1937); A. Brin, C. R. Acad. Sci. (Paris) **238**, 1022 (1954); A. Brin and R. Merigoux, *ibid.* **238**, 1808 (1954).

[3]D. Beysens and C. M. Knobler, Phys. Rev. Lett. **57**, 1433 (1986).

[4]J. W. Rose and L. R. Glicksman, Int. J. Heat Mass Transfer

16, 411 (1973).
[5]J. -L. Viovy, D. Beysens, and C. M. Knobler, Phys. Rev. A **37**, 4965 (1988).
[6]P. Meakin and F. Family, J. Phys. A **22**, L225 (1989).
[7]D. Fritter, C. M. Knobler, D. Roux, and D. Beysens, J. Stat. Phys. **52**, 1447 (1988).
[8]T. Rogers, K. R. Elder, and R. C. Desai, Phys. Rev. A **38**, 5303 (1988).
[9]D. Beysens, C. M. Knobler, and H. Schaffar, Phys. Rev. B **41**, 9814 (1990).
[10]C. M. Knobler and D. Beysens, Europhys. Lett. **6**, 707 (1988).
[11]F. Perrot and D. Beysens, Rev. Sci. Instrum. **58**, 183 (1987).
[12]J. Sagiv, J. Am. Chem. Soc. **102**, 92 (1980).
[13]D. Beysens, D. Fritter, D. Roux, C. M Knobler, and J. -L. Viovy, in *Proceedings of the International Symposium on Dynamics of Ordering Processes in Condensed Matter,* edited by S. Komura and H. Furukawa (Plenum, Kyoto, 1988), p. 403.
[14]F. Kreith, *Principles of Heat Transfer,* 3rd ed. (Harper and Row, San Francisco, 1973).
[15]In analogy to heat transfer, see R. J. Nickerson, in *Developments in Heat Transfer,* edited by W. M. Rohsenow, (MIT Press, Cambridge, MA, 1964), p. 37.
[16]L. E. Sissom and D. R. Pitts, *Elements of Transport Phenomena* (McGraw-Hill, San Francisco, 1972), p. 522.
[17]H. H. Sogin, Trans. ASME **80**, 61 (1958).
[18]E. E. Gose, A. N. Mucciardi, and E. Baer, Int. J. Heat Mass Transfer **10**, 15 (1967).
[19]I. Tanasawa and F. Tachibana, in *Proceedings of the Fourth International Heat Transfer Conference,* edited by U. Grigull and E. Hahne (Elsevier, Amsterdam, 1970), Vol. 6.
[20]L. R. Glicksman and A. W. Hunt, Jr., Int. J. Heat. Mass Transfer **15**, 2251 (1972).
[21]R. Vincent, Proc. R. Soc. London Ser. A **321**, 53 (1971).
[22]B. J. Briscoe and K. P. Galvin, J. Phys. D **23**, 422 (1990).
[23]F. Family and P. Meakin, Phys. Rev. Lett. **61**, 428 (1988).
[24]A. Steyer, P. Guenoun, D. Beysens, D. Fritter, and C. M. Knobler, Europhys. Lett. **12**, 211 (1990).
[25]E. L. Hinrichsen, J. Feder, and T. Jossang, J. Stat. Phys. **44**, 793 (1986).
[26]E. B. Fowlkes, J. Am. Stat. Assoc. **74**, 561 (1979).
[27]R. Hosemann and S. N. Bagchi, *Direct Analysis of Diffraction by Matter* (Interscience, New York, 1962), Chap. 11.

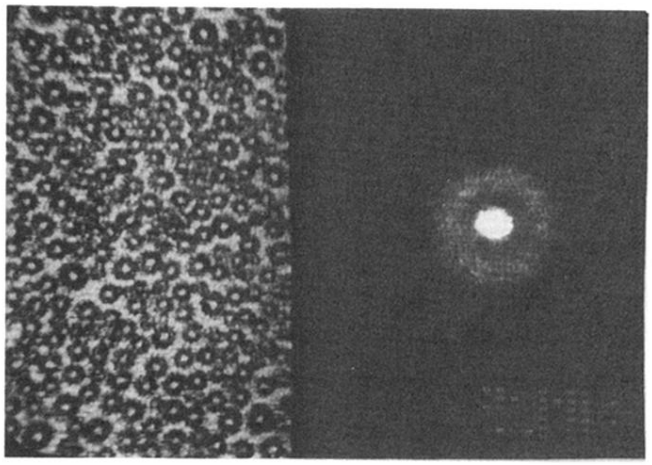

FIG. 1. Photos of BF growth: self-similar stage (ii), where the pattern of droplets is shown on the left and the annular light scattering pattern is on the right.